MATER. RES. LETT.
2019, VOL. 7, NO. 5, 180–187
https://doi.org/10.1080/21663831.2019.1572663

Nano-scale Si segregation and precipitation in $Cr_2Al(Si)C$ MAX phase coatings impeding grain growth during oxidation

K. G. Pradeep[a], K. Chang[a], A. Kovács[b], S. Sen[a], A. Marshal[a], René de Kloe[c], R. E. Dunin-Borkowski[b] and J. M. Schneider[a]

[a]Materials Chemistry, RWTH Aachen University, Aachen, Germany; [b]Ernst Ruska-Centre for Microscopy and Spectroscopy with Electrons and Peter Grünberg Institute, Jülich, Germany; [c]EDAX, Tilburg, The Netherlands

ABSTRACT

We recently reported that the columnar grain width of Cr_2AlC MAX phase coatings increases during oxidation (4 h at 1120°C) by 80%, while for 0.7 at.% Si additions to Cr_2AlC, coarsening of only 12% was observed. Here, we use nm scale compositional and microstructural investigations to identify significant differences between Cr_2AlC and $Cr_2Al(Si)C$. In particular, needle-shaped precipitates coarsen into globular Cr_3Si precipitates upon oxidation in the Si-containing MAX phase. We infer that the presence of these precipitates, which are located predominantly along grain boundaries in the MAX phase, retards coarsening during oxidation by Zener pinning.

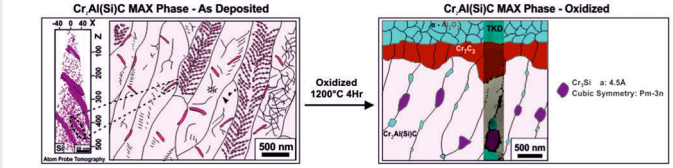

IMPACT STATEMENT

This is the first report of Zener pinning in MAX phases. We show that Si additions to Cr_2AlC cause the formation of precipitates, which retard grain coarsening during oxidation.

ARTICLE HISTORY
Received 20 October 2018

KEYWORDS
MAX phases; self-healing; precipitate; grain boundary; Zener pinning

Introduction

Cr_2AlC belongs to the subset of ternary metal carbides that have the general formula $M_{n+1}AX_n$ and are referred to as MAX phases (M: early transition metal; A: A group element; X: C or N) [1–3]. MAX phases typically exhibit nano-laminated structures with modulated charge density distributions, in which M-X layers (ionic - covalent bonds) are separated by A layers (metallic bonds). As a result, they possess both metallic and ceramic properties [1,2,4]. The potential for utilizing MAX phase ceramics (especially Ti_3AlC_2, Ti_2AlC and Cr_2AlC) as self-healing materials has been investigated in recent years. In these materials, the products of oxidation, especially, α-Al_2O_3 and other oxides have been shown to fill crack sites, thereby effectively healing them [5–8]. Song et al. [5] investigated the mechanical properties of the self-healed Ti_3AlC_2 MAX phase and reported that after oxidation, a crack-healed zone consisted primarily of α-Al_2O_3, in addition to minor distributions of TiO_2. However, it was proposed that the formation of less protective and relatively weak TiO_2 needs to be avoided, in order to achieve better mechanical properties [5,9].

The quest for the development of self-healing MAX phase materials that produce only α-Al_2O_3 along a crack zone after high temperature oxidation has directed research towards the study of Cr_2AlC [10–14]. Yang et al. [8] investigated the oxidation kinetics of bulk Cr_2AlC at 1100°C for 40 h. They reported that the diffusion of Al along oxide grain boundaries dominated the self-healing kinetics. These results suggest that α-Al_2O_3 scale formation on Cr_2AlC is comparable to that on other Al-containing high temperature materials, such as nickel and titanium aluminides [15]. However, the oxidation kinetics is sluggish. For efficient healing of macroscopic cracks, for example to impede erosive wear, fast crack healing and hence an increased oxidation rate are required.

CONTACT K. G. Pradeep kgprad@gmail.com Materials Chemistry, RWTH Aachen University, Kopernikusstrasse 10, 52074, Aachen, Germany

Supplemental data for this article can be accessed here. https://doi.org/10.1080/21663831.2019.1572663

We recently showed that the addition of Si as a fourth alloying element in the minor amount of 0.7 at.% (determined by energy-dispersive X-ray spectroscopy (EDX)) to the Cr_2AlC MAX phase can enhance the Al_2O_3 layer thickness by ~40% upon oxidation at 1120°C in air for 4 h [16,17]. It was also observed that the $Cr_2Al(Si)C$ MAX phase exhibited retarded grain growth during oxidation. Detailed near atomic-scale characterization using atom probe tomography (APT) did not reveal the presence of Si, even in trace amounts, either in the Al_2O_3 layer or in the chromium carbide layer located immediately below the Al_2O_3 layer. However, APT revealed the incorporation of up to 1.3 ± 0.2 at.% Si into the MAX phase after oxidation [16]. Hence, the role of Si in the retardation of MAX phase grain growth is currently not understood.

Here, we investigate the role of the addition of 0.7 at.% Si on phase formation and nanostructure evolution during annealing in the Cr_2AlC MAX phase using Scanning Transmission Electron Microscopy (STEM), APT and Transmission Kikuchi Diffraction (TKD).

Methods

MAX phases of Cr_2AlC and $Cr_2Al(Si)C$ with 0.7 at.% Si were synthesized using DC magnetron sputtering in an industrial chamber (CC800/9, Cemecon AG, Germany). Further synthesis details can be found in Ref [16]. Oxidation was performed using a Carbolite HTF-1700 laboratory furnace at 1120°C for 4 h in air.

A probe-aberration corrected FEI Titan 80–200 transmission electron microscope equipped with in-column EDX detectors was used to record elemental distributions across different regions of the MAX phase coatings, both in the as-deposited and in the oxidized states. High-angle annular dark-field (HAADF) STEM images were recorded together with the EDX maps to correlate the structure and chemical composition. Further details about the microscope can be found in Ref. [18].

Sample preparation for STEM, TKD analysis, EDX mapping and APT was performed using an FEI Helios Nanolab 660 dual-beam system following the procedures that are described elsewhere [19–21]. APT tips were aligned along the growth direction of the as-deposited film. APT measurements were performed in laser-pulsed mode, with applied laser energy of 30 pJ at 250 kHz repetition rates, using a local electrode atom probe (LEAP 4000X HR) system from CAMECA Instruments. Tips were maintained at 60 K during the measurements. Data reconstruction and analysis were performed using IVAS 3.6.10a software.

TKD phase and orientation data were collected using an EDAX TEAM^{TM} Pegasus EDS-EBSD system equipped with a HIKARI Plus electron backscatter diffraction detector. Analysis of the TKD-generated data was performed using EDAX OIM^{TM} Analysis 8 software.

Results and discussion

X-ray diffraction patterns recorded from the as-deposited Cr_2AlC and $Cr_2Al(Si)C$ MAX phase samples indicate that phase-pure MAX phases were obtained for both compositions (Figure S1). The differences in

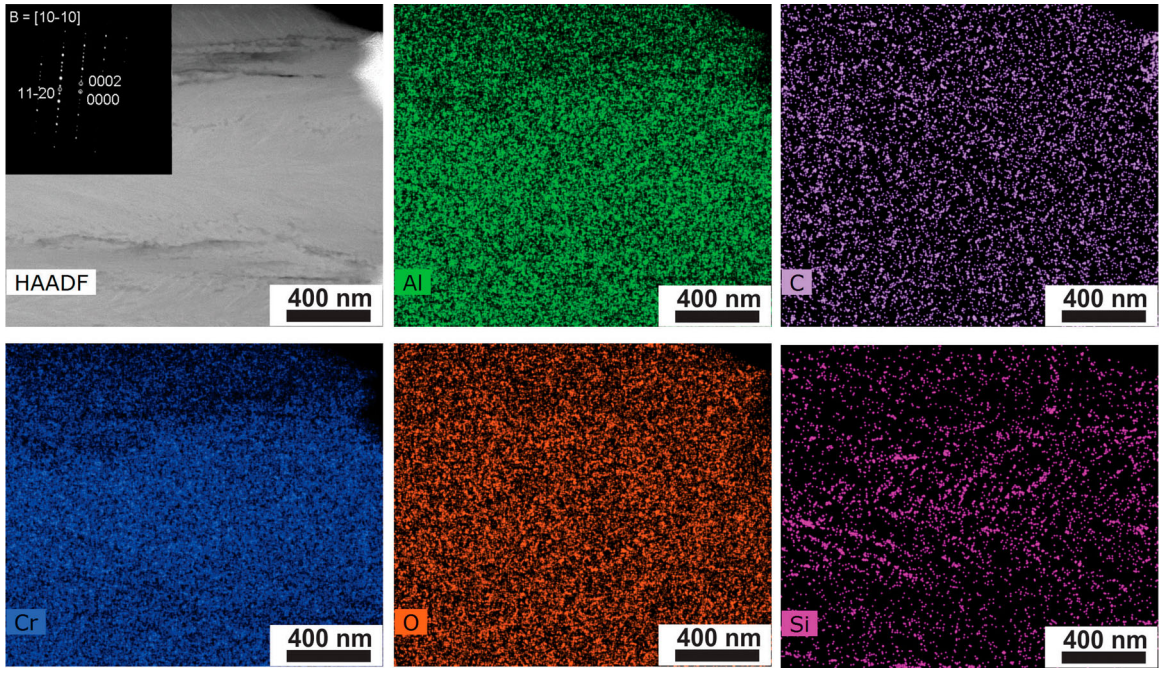

Figure 1. STEM-HAADF image of the as-deposited $Cr_2Al(Si)C$ MAX phase coating with an SAED pattern inset and corresponding elemental maps of Al, C, Cr, O and Si extracted from EDX measurement.

diffraction peak intensities corresponding to Cr_2AlC and $Cr_2Al(Si)C$ indicate that both coatings grow with different textures.

Figure 1 shows the nanostructure and the elemental distribution of the $Cr_2Al(Si)C$ MAX phase in the STEM-HAADF image and corresponding EDX maps. Comparable to the Cr_2AlC MAX phase sample (Figure S2), 'V shaped' defects are observed in the columnar MAX phase grains, with elemental maps of Cr, Al, C and O showing uniform and random distributions (see Figure 1). However, the Si distribution is non-uniform, with Si segregating to the 'V-shaped' defects. A selected-area electron diffraction (SAED) pattern (inset of Figure 1) recorded from a sample with an identical chemical composition to that reported in Ref. [16] was consistent with the formation of the $Cr_2Al(Si)C$ MAX phase.

In order to quantify the local composition of the segregated regions, APT measurements were performed on the same as-deposited $Cr_2Al(Si)C$ MAX phase sample as was utilized for the STEM/EDX investigations. Three-dimensional elemental distribution maps of each of the constituent elements along the growth direction of the film are shown in Figure S3. Si and O show strong local variations in concentration.

In order to analyse the spatial variation in the Si concentration further, a 10 at.% Si iso-concentration surface was used to distinguish between Si in the MAX phase matrix and the Si-enriched needle-shaped regions, as shown in Figure 2. A proximity histogram obtained from interface 1 indicates the presence of a $\sim$10 nm thick precipitate with approximate composition Cr_5Si_3C. In contrast, a proximity histogram obtained from interface 2 indicates the presence of a $\sim$5 nm thick precipitate with approximate composition Cr_3Si. The minimum length of the precipitates is on the order of 250 nm, although it should be taken into consideration that the APT tip volume is limited. It can also be inferred from the proximity histograms that Si shows a solubility of up

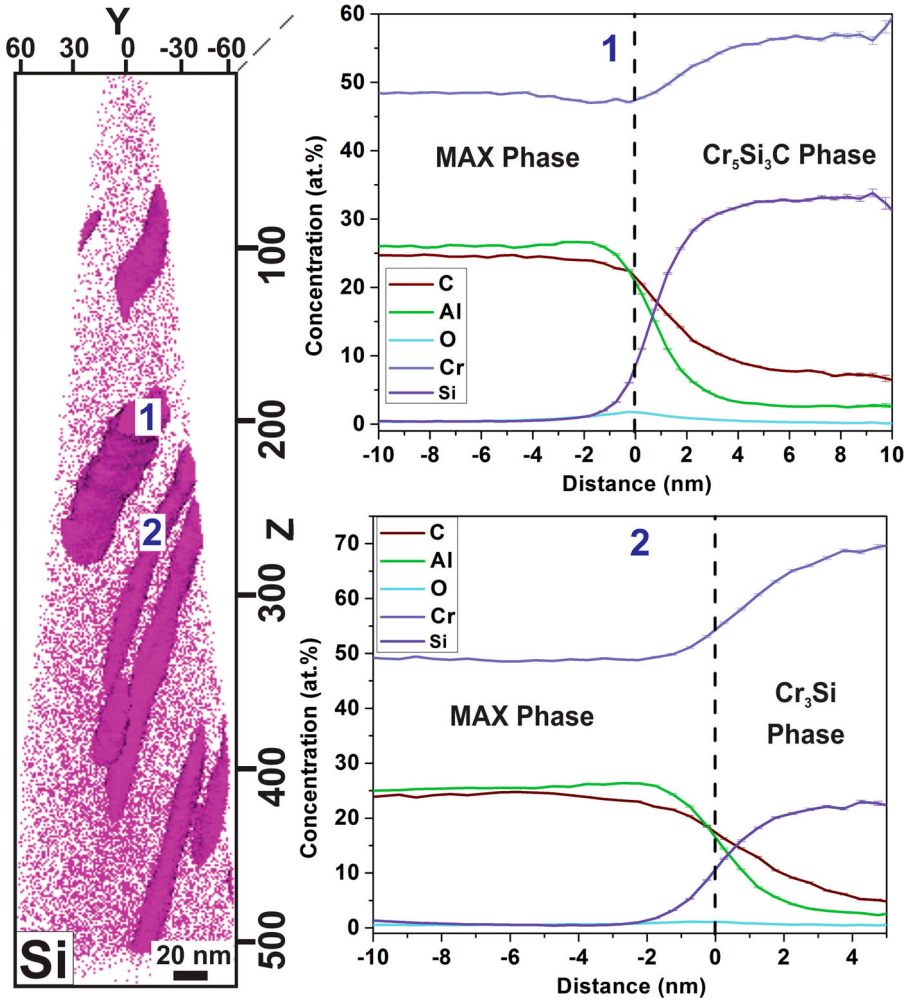

Figure 2. Three-dimensional elemental distribution map of Si in the as-deposited $Cr_2Al(Si)C$ MAX phase coating, with the Si-enriched regions delineated by a 10 at.% isoconcentration surface. Proximity histograms taken along interfaces 1 and 2 using a 0.5 nm bin width are shown on the right.

to 0.5 ± 0.02 at.% in the MAX phase matrix. It should be noted that the formation of segregations (identified using STEM-EDX in Figure 1) and precipitations (identified using APT in Figure 2 and S3) is not reflected in the XRD data (Figure S1). Although the segregations may or may not be crystalline, the volume fraction of the precipitations may be too small to be detected using XRD (assuming that they are crystalline). Furthermore, no positive phase identification of the precipitates could be obtained using SAED [16]. The Si rich precipitations, which have a thickness of $\sim$5–10 nm and a length on the order of 250 nm, should be visible using TEM and hence should be detectable using SAED. Furthermore, the observation of trace Si segregation along the 'V shaped' defect sites in Figure 1, without appreciable Cr or C enrichment, suggests that these segregations are different to the precipitations observed using APT (with Cr or C enrichment). It may therefore be speculated that preferential FIB milling of these precipitations (possibly along grain boundaries) occurred during TEM specimen preparation, thereby excluding them from SAED diffraction analysis. Evidence in support of this hypothesis is provided by the observation of 50–80 nm wide and 800 nm – 2 µm long regions of material loss (continuous void formation) along specific grain boundary regions from the TEM lamella used for imaging the as-deposited $Cr_2Al(Si)C$ MAX phase sample (see Figure 5 in Ref. [16]). The size (50–80 nm wide) of these regions approximately resembles the size of the precipitates observed in Figure 2 and Figure S3.

In an effort to image Si segregations and Si precipitations in one sample, STEM imaging and EDX mapping were performed on an APT tip prepared from the as-deposited $Cr_2Al(Si)C$ MAX phase sample, as shown in Figure S4. The STEM HAADF image shows contrast variations that may be, at least in part, due to variations in atomic number (Z) of the (segregated) elements that are present in the imaged volume. In addition to Z-contrast, diffraction contrast arising from the potentially nanocrystalline nature of the sample may be present. Corresponding EDX elemental maps reveal a Si distribution that is similar in morphology (thickness and length) to the Si-rich precipitations observed using APT in Figure 2.

It should be noted that the impurity O concentrations in both the Si rich precipitations and the matrix MAX phase regions, as observed in the proximity histograms shown in Figure 2, are $\leq 0.44 \pm 0.01$at. %. The local O enrichment seen in Figure S3 corresponds to enrichment in O up to a concentration of 1.12 ± 0.02 at.% at the interface between the Si-rich precipitates and the MAX phase, as observed in the proximity histograms shown in Figure 2. Interestingly, such O segregation is not observed in the Cr_2AlC MAX phase sample, even along the 'V-shaped' defects in Figure S2.

Hence, no segregation or significant spatial distribution in chemical composition could be identified in the Cr_2AlC coating. However, the Si-containing films exhibit Si segregations and precipitations, as discussed above. It was previously observed that a $Cr_2Al(Si)C$ MAX phase

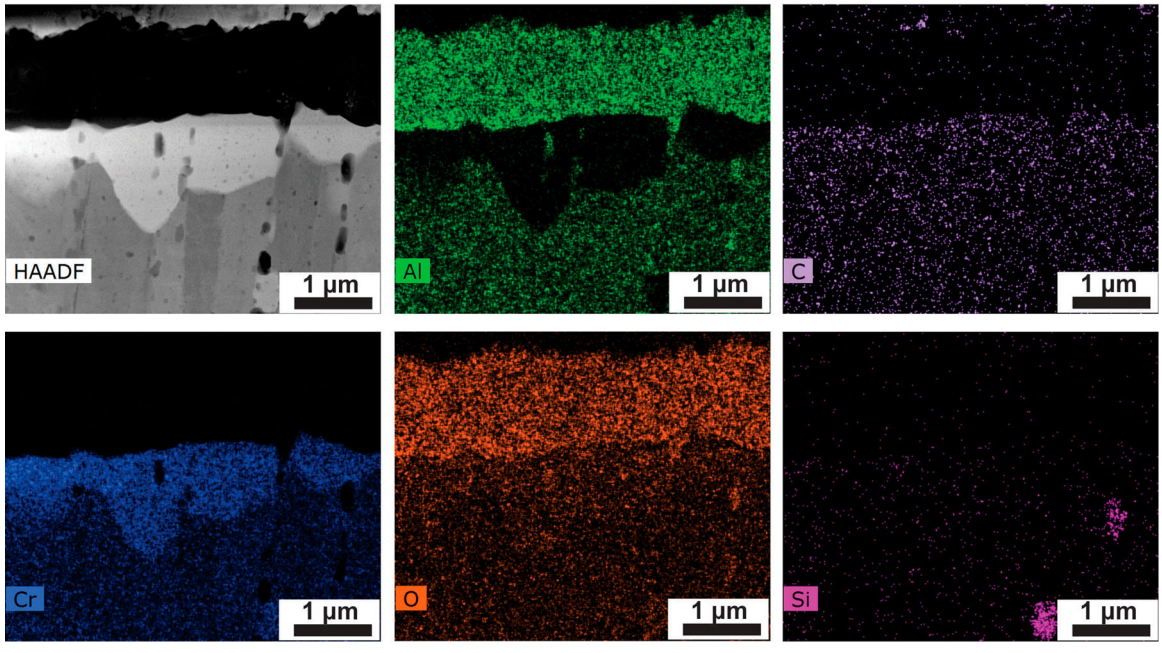

Figure 3. STEM-HAADF image of the 1120°C 4 h oxidized $Cr_2Al(Si)C$ MAX phase and corresponding elemental maps of Al, C, Cr, O and Si extracted from EDX measurement.

retarded grain growth during oxidation at 1120°C for 4 h in air [16]. In order to obtain a comparison with the as-deposited state, STEM-EDX analysis was performed on the oxidized $Cr_2Al(Si)C$ MAX phase sample, as shown in Figure 3. The presence of Al_2O_3 and Cr_7C_3 layers can be inferred from the observed enrichment of Al and Cr in the elemental maps. The absence of Si in these layers is consistent with previously reported APT observations [16].

In contrast to the as-deposited state, distinct regions where Al and Si are separately enriched can be observed along the grain boundaries of the parent MAX phase. The Al-enriched regions are associated with an increased O concentration. Hence, these local precipitations along the grain boundaries appear to be alumina. It is reasonable to assume that the formation of Al_2O_3 particles along the MAX phase grain boundaries is a consequence of O inward diffusion during the oxidation process [8] and diffusion of O that was incorporated from the residual gas during sputtering [22]. Similarly, the regions that are enriched in Si are also located along the grain boundaries and are characterized by an increase in Cr concentration.

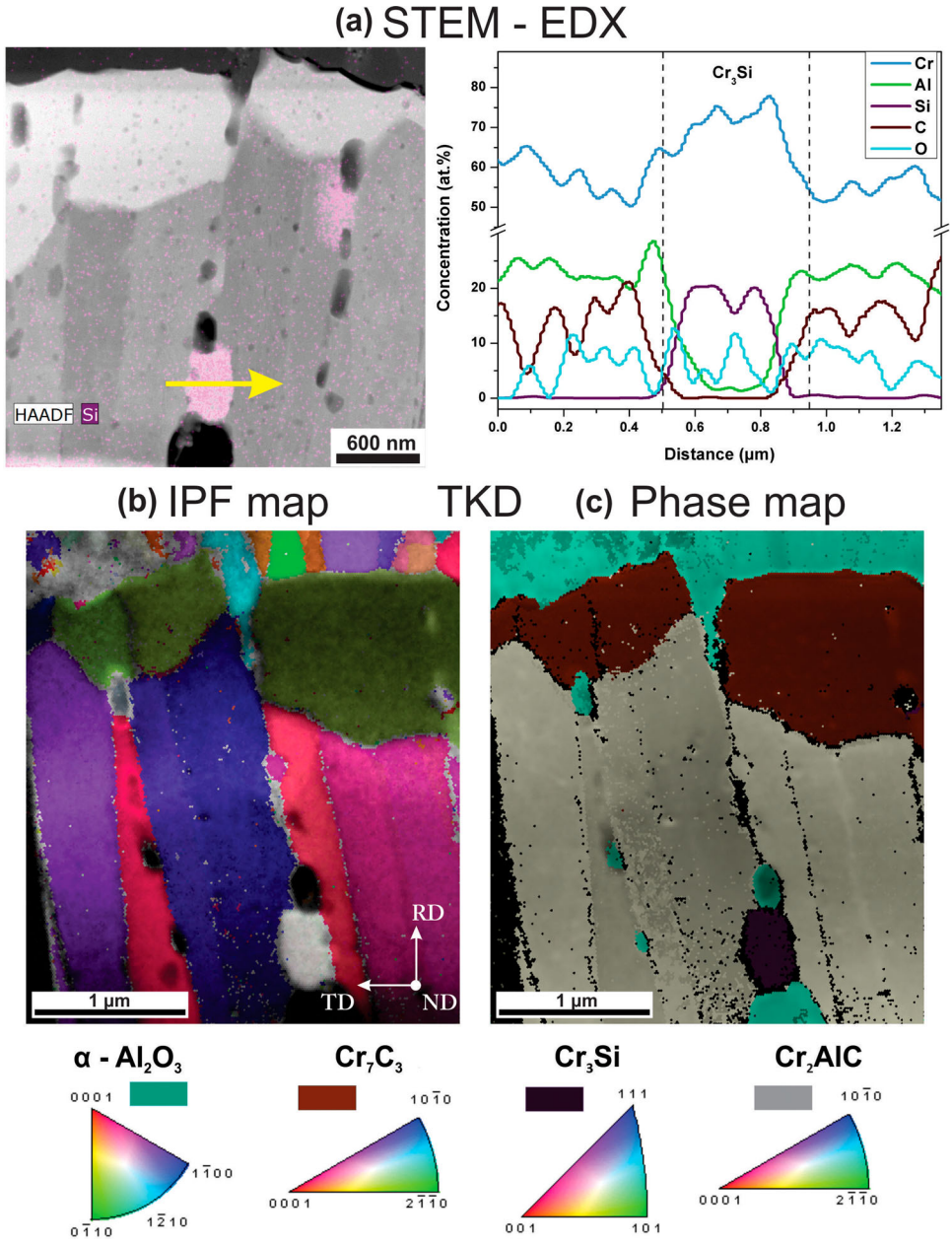

Figure 4. Correlative analysis of the 1120°C 4 h oxidized $Cr_2Al(Si)C$ MAX phase coating (a) STEM-HAADF image overlaid with the Si elemental map and corresponding 1-dimensional concentration profile taken along the Si-rich precipitate indicated by the yellow arrow. (b) Transmission Kikuchi diffraction inverse pole figure map and (c) the corresponding phase map showing the presence of cubic Cr_3Si precipitates along the hexagonal-close-packed MAX phase grain boundaries.

When compared with the local composition analysis carried out on the as-deposited samples, the needle-shaped precipitations have coarsened significantly (from ~5–10 nm in diameter in the as-deposited state) to domains of ~500 nm in diameter. A 1-dimensional concentration profile obtained along a Si-rich precipitate (indicated by a yellow arrow in Figure 4(a)) is consistent with a Cr_3Si stoichiometry. In order to complete the investigation of the local composition with structural information, correlative TKD measurements were performed on the same sample that was used for STEM-EDX mapping (Figure 3). The results are shown in Figure 4(b) and (c). The microstructure of the oxidized $Cr_2Al(Si)C$ MAX phase sample along the cross-section is shown in the form of a map that indicates the crystallographic direction normal to the thin film and the oxide scale growth directions using inverse pole figure (IPF) colors in Figure 4(b). In the phase map shown in Figure 4(c), columnar MAX phase grains, which have a column diameter of ~100–300 nm, are visible under a ~700 nm thick Cr_7C_3 layer and the α-Al_2O_3 layer. A cubic Cr_3Si globular precipitate phase (a = 4.5 Å; purple color) is visible along the columnar MAX phase grain boundary.

Based on the measurement of local composition and microstructure presented above, a schematic representation of the oxidation-induced changes in morphology of Cr_2AlC and $Cr_2Al(Si)C$ is shown in Figure 5. Significant coarsening is observed for the Cr_2AlC MAX phase grains [16] after oxidation for 4 h at 1120°C. For the Si-containing Cr_2AlC, coarsening is retarded [16]. Based on the observation of Si segregation at 'V-shaped' defects and the presence of Si-rich precipitates with approximate compositions Cr_3Si and Cr_5Si_3C located along grain boundaries, we infer that these precipitations hinder grain growth by Zener pinning. The grain boundary mobility of the $Cr_2Al(Si)C$ MAX phase sample appears to be significantly reduced due to the presence of the Si-rich precipitations, resulting in retarded coarsening.

In order to further elucidate the effect of Zener pinning on MAX phase grain growth, the temporal evolution of the 1 at.% Si containing Cr_2AlC MAX phase columnar width during oxidation in air at 1100°C for up to 240 min is compared with Si free Cr_2AlC MAX phase. The corresponding results are displayed in Figure 6, where it is shown that the addition of 1 at.% Si to Cr_2AlC MAX phase retards grain growth significantly compared

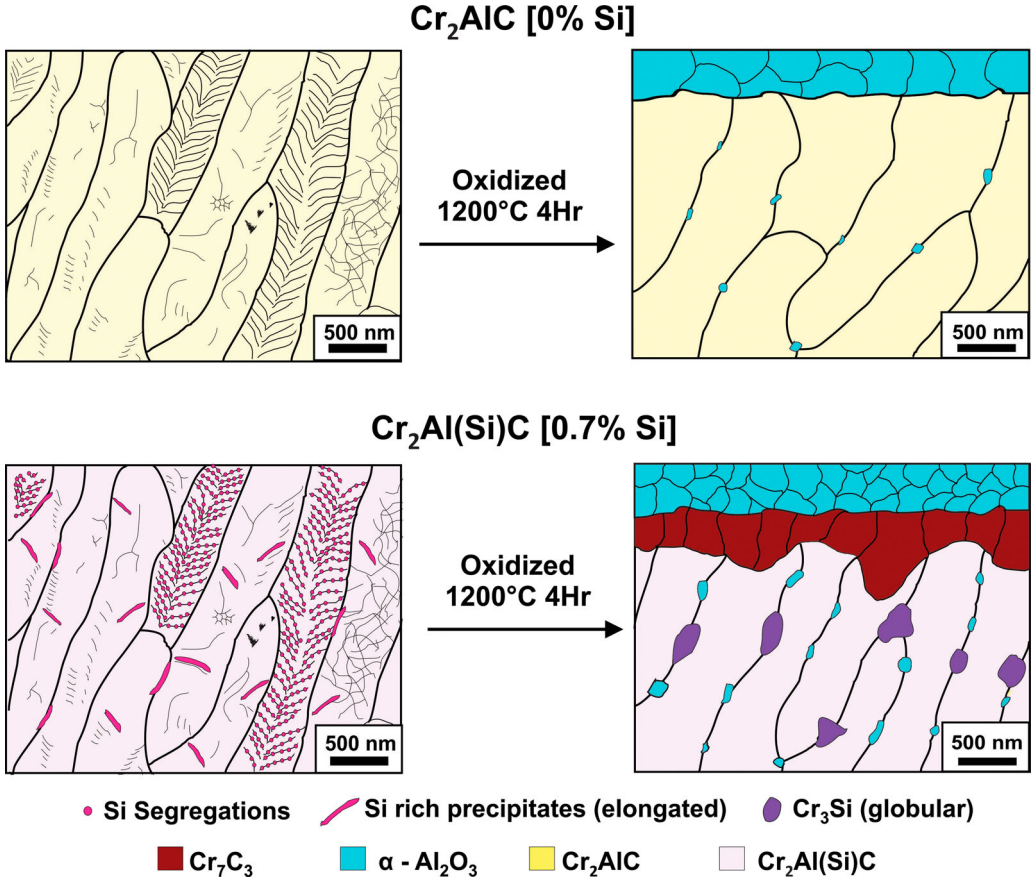

Figure 5. Schematic representations of oxidation-induced changes in the morphology of the Cr_2AlC and $Cr_2Al(Si)C$ coatings. The as-deposited morphologies are compared to those obtained after oxidation for 4 h at 1120°C.

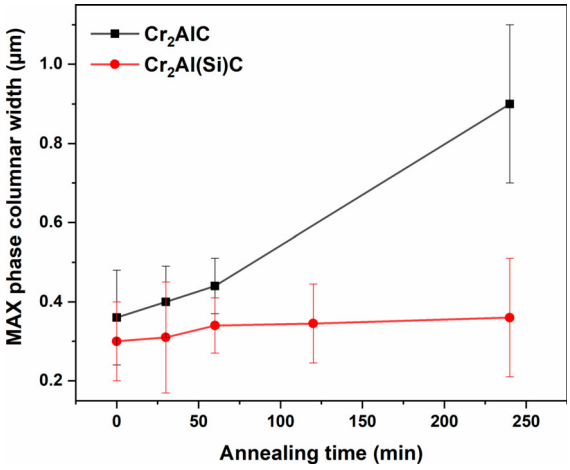

Figure 6. Variation in columnar grain width as a function of annealing time for Cr_2AlC and 1 at.% Si added $Cr_2Al(Si)C$ MAX phases annealed at 1100°C in air.

to the Si free Cr_2AlC MAX phase. These data underline that Zener pinning defines the high temperature behavior of Si containing MAX phases during high temperature exposure.

Conclusions

We have studied phase formation and nanostructure evolution in as-deposited and oxidized (at 1120°C for 4 h in air) MAX phase samples of Cr_2AlC and 0.7 at.% Si containing $Cr_2Al(Si)C$. Si was observed to segregate at 'V-shaped' growth defects in the MAX phase grains, in addition to being incorporated in the form of Cr_3Si and Cr_5Si_3C needle-shaped precipitations, which are located preferentially along grain boundaries in the as-deposited $Cr_2Al(Si)C$ MAX phase. Upon oxidation at 1120°C for 4 h in air, the needle-shaped (~5–10 nm diameter) Cr_3Si precipitates were observed to undergo significant coarsening into a globular morphology (~500 nm in diameter), accompanied by annihilation of the Si-enriched 'V-shaped' growth defects. TKD measurements confirmed the presence of cubic Cr_3Si (a = 4.5 Å) precipitates along the grain boundaries of the Si-containing MAX phase. In comparison to the Cr_2AlC MAX phase (without Si additions) which shows an 80% increase in columnar grain width upon oxidation, coarsening of the $Cr_2Al(Si)C$ MAX phase upon oxidation was retarded to only 12%. This difference by a factor of 6.7 in the coarsening behavior is attributed to Zener pinning of grain boundaries by the Si-containing precipitates.

Acknowledgments

The authors gratefully acknowledge financial support from the German Research Foundation (DFG) within SPP 1568. Dr. Lin Shang is acknowledged for providing the as-deposited and 1120°C 4 h oxidized samples investigated in the present study. Jochen M. Schneider gratefully acknowledges financial support from the MPG fellow program.

Disclosure statement

No potential conflict of interest was reported by the authors.

Funding

This work was supported by Deutsche Forschungsgemeinschaft [Grant Number SPP 1568].

References

[1] Barsoum MW. The $M_{N+1}AX_N$ phases: a new class of solids; thermodynamically stable nanolaminates. Prog Solid State Chem. 2000;28:201–281.
[2] Music D, Schneider JM. The correlation between the electronic structure and elastic properties of nanolaminates. JOM. 2007;59:60–64.
[3] To Baben M, Music D, Emmerlich J, et al. Extending the rule of mixture to the sub unit-cell level. Scr Mater. 2011;65:735–738.
[4] Barsoum MW, Zhen T, Kalidindi SR, et al. Fully reversible, dislocation-based compressive deformation of Ti_3SiC_2 to 1 GPa. Nat Mater. 2003;2:107–111.
[5] Song GM, Pei YT, Sloof WG, et al. Oxidation-induced crack healing in Ti_3AlC_2 ceramics. Scr Mater. 2008;58:13–16.
[6] Yang HJ, Pei YT, et al. High temperature healing of Ti_2AlC: On the origin of inhomogeneous oxide scale. Scr Mater. 2011;65:135–138.
[7] Yang HJ, Pei YT, Rao JC, et al. Self-healing performance of Ti_2AlC ceramic. J Mater Chem. 2012;22:8304–8313.
[8] Yang HJ, Pei YT, De Hosson JTM. Oxide-scale growth on Cr_2AlC ceramic and its consequence for self-healing. Scr Mater. 2013;69:203–206.
[9] Li S, Song G, Kwakernaak K, et al. Multiple crack healing of a Ti_2AlC ceramic. J Eur Ceram Soc. 2012;32:1813–1820.
[10] Lee DB, Nguyen TD, Han JH, et al. Oxidation of Cr_2AlC at 1300°C in air. Corros Sci. 2007;49:3926–3934.
[11] Lee DB, Park SW. Oxidation of Cr_2AlC between 900 and 1200°C in air. Oxid Met. 2007;68:211–222.
[12] Lee DB, Nguyen TD, Park SW. Long-time oxidation of Cr_2AlC between 700 and 1000°C in air. Oxid Met. 2012;77:275–287.
[13] Hajas DE, To Baben M, et al. Oxidation of Cr_2AlC coatings in the temperature range of 1230 and 1410°C. Surf Coat Technol. 2011;206:591–598.
[14] Li S, Xiao L, Song G, et al. Oxidation and crack healing behavior of a fine-grained Cr_2AlC ceramic. J Am Ceram Soc. 2013;96:892–899.
[15] Brumm MW, Grabke HJ. The oxidation behaviour of NiAl-I. phase transformations in the alumina scale during oxidation of NiAl and NiAl-Cr alloys. Corros Sci. 1992;33:1677–1690.
[16] Shang L, Konda Gokuldoss P, et al. Effect of Si additions on the Al_2O_3 grain refinement upon oxidation of Cr_2AlC MAX phase. J Eur Ceram Soc. 2017;37:1339–1347.

[17] Shang L, Music D, Baben MT, et al. Phase stability predictions of $Cr_{1-x},M_x)_2(Al_{1-y},A_y)(C_{1-z},X_z)$ (M = Ti, Hf, Zr; A = Si, X = B). J Phys D: Appl Phys. 2014;47:065308.
[18] FEI Titan G2 800-200 CREWLEY. Ernst ruska-center for microscopy and spectroscopy with electrons (ER-C). J Large-Scale Res Facil. 2016;2:A43.
[19] Mandal S, Pradeep KG, Zaefferer S, et al. A novel approach to measure grain boundary segregation in bulk polycrystalline materials in dependence of the boundaries' five rotational degrees of freedom. Scr Mater. 2014;81:16–19.
[20] Zhang H, Pradeep KG, et al. Dynamic strain-induced transformation: An atomic scale investigation. Scr Mater. 2015;109:23–27.
[21] Basu I, Pradeep KG, et al. The role of atomic scale segregation in designing highly ductile magnesium alloys. Acta Mater. 2016;116:77–94.
[22] Schneider JM, et al. On the effect of hydrogen incorporation in strontium titanate layers grown by high vacuum magnetron sputtering. Appl Phys Lett. 1999;75(22): 3476–3478.